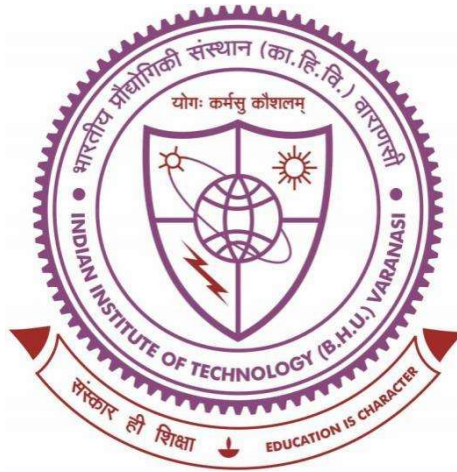


# Formulation and Evaluation of Methotrexate-loaded Polymeric Nanoparticles in Breast Cancer Treatment



Thesis submitted in partial fulfilment  
For the Award of Degree  
**Doctor of Philosophy**

BY

**RINKI VERMA**

SCHOOL OF BIOMEDICAL ENGINEERING  
INDIAN INSTITUTE OF TECHNOLOGY BHU, VARANASI, 221005, U.P.,  
INDIA

Roll No. 18021005

2023

## CERTIFICATE

It is certified that the work contained in this thesis entitled " **Formulation and Evaluation of Methotrexate-loaded Polymeric Nanoparticles in Breast Cancer Treatment** " by **Rinki Verma** has been carried out under my supervision, and it has not been submitted elsewhere for a degree.

It is further certified that **Rinki Verma** has fulfilled all the Comprehensive Examination, Candidacy, and SOTA requirements for the award of Ph.D. Degree.



**Dr. Manoj Kumar**  
(Supervisor)

Department of Chemical Engineering & Technology,  
Indian Institute of Technology,  
Banaras Hindu University  
Varanasi-221005, India

Dr. MANOJ KUMAR  
Associate Professor  
Department of Chemical Engg. & Techn.  
IIT (BHU), Varanasi-221005

## DECLARATION BY THE CANDIDATE

I, Rinki Verma, certify that the work embodied in this thesis is my own bonafide work and carried out by me under the supervision of Dr. Manoj Kumar for a period from July 2018 to July 2023, at the School of Biomedical Engineering, India Institute of Technology (Banaras Hindu University), Varanasi 221005, UP, India. The matter embodied in this thesis has not been submitted for the award of any other degree/diploma. I declare that I have faithfully acknowledged and given credits to the research worker wherever their works have been cited in this thesis. I further declare that I have not willfully copied any other's work, paragraphs, text, data, results, etc., reported in the journal, books, magazines reports, dissertations, thesis, etc., or available at websites and have not included in this thesis and have not cited as my work.

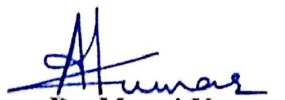
Date: 19-07-2023

Place: IIT (BHU), Varanasi

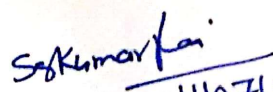
  
Rinki Verma

## CERTIFICATE BY THE SUPERVISOR

It is certified that the above statements made by the students are correct to the best of my knowledge.

  
Dr. Manoj Kumar  
(Supervisor)

Department of Chemical Engineering & Technology,  
Indian Institute of Technology,  
Banaras Hindu University  
Varanasi-221005, India  
DR. MANOJ KUMAR  
Associate Professor  
Department of Chemical Engg. & Techn.  
IIT (BHU), Varanasi-221005

  
Signature 11/07/23  
Coordinator of the School  
समन्वयक/CO-ORDINATOR  
जैव चिकित्सा अभियांत्रिकी स्कूल  
SCHOOL OF BIOMEDICAL ENGINEERING  
भारतीय प्रौद्योगिकी संस्थान (का.हि.)  
INDIAN INSTITUTE OF TECHNOLOGY (B.H.U.)  
वाराणसी 221005/VARANASI-221005

## COPY RIGHT TRANSFER CERTIFICATE

Title of thesis: "Formulation and Evaluation of Methotrexate-loaded Polymeric Nanoparticles in Breast Cancer Treatment".

Candidate's name: **Rinki Verma**

### Copyright Transfer

The undersigned hereby assigns to the Indian Institute of Technology (Banaras Hindu University), Varanasi – 21005, India, all right under the copyright that may exist in and for the above thesis submitted for the award of the doctor of philosophy.

Date: 19-07-2023  
Place: IIT (BHU), Varanasi  
Verma)

  
(Rinki

**Note:** However, the author may reproduce or authorize others to reproduce material extracted verbatim from the thesis, or derivative of the thesis for the author's personal use, provided that the source and the institute's copyright notice are indicated

---

## ACKNOWLEDGEMENT

I am greatly indebted to my honored, respected supervisor, **Dr. Manoj Kumar**, Associate professor, at the Department of Chemical Engineering, India Institute of Technology (Banaras Hindu University) Varanasi 221005, UP, India, for his guidance and support. He allowed me to explore independently, taught me how to question thoughts and express ideas, and helped me recover when my steps faltered. I thank him for the continuous support of my Ph.D. study and research and his patience, motivation, enthusiasm, and immense knowledge. I am grateful to him for holding me to a high research standard and enforcing strict validations for each research result, thus teaching me how to do research. Your advice in both research and my carrier have been priceless.

Further, I am very thankful to **Dr. Sanjeev Kumar Mahto**, Coordinator, School of Biomedical Engineering, who encouraged my research and grew as a research scientist.

I would also like to thank my Research Progress Evaluation Committee member, **Dr. Sanjay Singh Rai**, Associate Professor at the School of Biomedical Engineering, India Institute of Technology (Banaras Hindu University), Varanasi 221005, UP, India, and **Dr. Gyan Prakash Modi**, Assistant professor at the Department of Pharmaceutical Engineering and Technology, India Institute of Technology (Banaras Hindu University), Varanasi 221005, UP, India for serving as my committee member even at hardship and for being my principal advisor. Their comments and suggestions during my work progress presentation improve the quality of my research work.

I also thank **Dr. Biplob Koch**, Department of Zoology, BHU, provided me with his lab facilities. I am thankful to **Professor S. Hemlata** (HOD), Department of Pharmaceutics Engineering and Technology, for allowing me to use the animal house central facility. I

---

am also thankful to **Dr. A.N Sahu** and **Dr. Ruchi Chawla** to provided me with their lab facilities.

I thank all the School of Biomedical Engineering professors for their advice and motivation. I would also like to be thankful to the School of Biomedical Engineering staff, who has been supportive in every way. I would also like to thank Mr. Barat Lal, technical staff at the School of Biomedical Engineering, for their help during my research. I sincerely thank the School of Biomedical Engineering, India Institute of Technology (Banaras Hindu University), Varanasi, which provided a platform for this research.

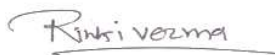
I am wholeheartedly thankful to my dear lab mates **Vivek Kumar Verma, Prachi Srivastava, Anshuman Singh, Shivesh Sabbarwal, and Virendra Singh**, with whom I shared the lab with many ups and downs. You all are the decisive reason for the beautiful workplace in the laboratory.

All my beautiful friends are entitled to my most profound admiration for their constant encouragement and support during all the ups and downs of this phase. Thanks to **Devdutt Sharma, Varsha Rani, and Dr. Kanchan Maurya**. You all made this journey equally comfortable and memorable. I am also very thankful to my juniors **Devadatta Mohapatra, Mohini Mishra, and Vivek Jaiswal** for their support.

I am also highly thankful to all non-teaching and laboratory staff of the school for their help and cooperation extended for the successful completion of the work.

I am also thankful to the staff member of the Central Instrumental Facility (CIF).

Lastly, I would like to thank all those volunteers who participated in this study.



Rinki Verma

<b>CONTENTS</b>
<i>Certificate</i>
<i>Declaration by the candidate &amp; certificate by the supervisor</i>
<i>Copyright transfer certificates</i>
<i>Acknowledgment</i>
<i>Table of contents</i>
<i>List of Figures</i>
<i>List of Tables</i>
<i>List of abbreviations</i>
<i>Preface</i>
<b>Introduction: Cancer &amp; Therapeutics</b>
1.1 Cancer
1.1a Types of cancer
1.1.b Epidemiology
1.2 Breast cancer
1.2.1 Histological subtype
1.2.2 Molecular subtypes
1.3 Common treatments for breast cancer
1.4 Methotrexate
1.5 Challenges in cancer treatment
1.6 Nanoparticles
1.6.1 Polymer-based drug nanocarriers
1.7 Chitosan
1.8 Chitosan nanoparticles synthesis methods
1.8.1 Ionic gelation method
1.8.2 Microemulsion method
1.8.3 Self-assembly
1.8.4 Polymerization
1.8.5 Covalent cross-linking
1.8.6 Precipitation
1.8.7 Spray Drying
1.9 Advantages of ionic gelation over other synthetic methods

<b>Chapter 2: Literature Review</b>
2.1 Overview
2.2 Role of nanotechnology in cancer diagnosis and therapy
2.3 Metallic nanoparticles as drug delivery system
2.4 Limitations of metal and metal oxide nanoparticles in cancer treatment
2.5 Metal Salt nanoparticles
2.5.1 Calcium carbonate nanoparticles (CaCO <sub>3</sub> -NPs)
2.6 Carbon-based nanoparticles (C-NPs)
2.6.1 Carbon nanotubes (CNT)
2.6.2 Graphene oxide (GO) nanoparticles as drug delivery system
2.7 Limitations of carbon-based nanoparticles in cancer treatment
2.8 Polymer nanoparticles (P-NPs)
2.9 Biopolymer nanoparticles
2.9.1 Chitosan
2.9.2 Chitosan nanoparticles (CS-NPs)
2.10 Advantages of chitosan nanoparticles over metal nanoparticles, metal oxide nanoparticles, and carbon-based nanoparticles in cancer treatment
2.11 Problem Statement & Objective of the Study
<b>Chapter 3: Development and Optimization of Methotrexate Chitosan Nanocarrier for Breast Cancer Treatment</b>
3.1 Introduction
3.2 Experiment Section
3.2.1 Preparation of MTX-encapsulated chitosan nanocarrier
3.2.2 Design of experiments (DOE)
3.2.2a Taguchi orthogonal array design
3.2.2b Statistical optimization and data analysis
3.2.2c Data analysis and validation
3.2.3 Characterization
3.2.3a Physiochemical characterization
3.2.3b Stability studies
3.2.4 <i>In-vitro</i> drug release
3.2.5 Animal and treatment protocol
3.2.5.1 <i>In-vivo</i> pharmacokinetic studies
3.2.5.1a High-performance liquid chromatography (HPLC)

3.2.6 Toxicity studies and histopathological examinations
3.3 Characterization and Property Evaluation
3.3.1 Validation of the statistical model
3.3.1a Normal probability plots
3.3.1b Main effect plot
3.3.2 Response surface analysis
3.3.2a Influence of independent parameters on particles size
3.3.2b Influence of independent parameters on encapsulation efficiency
3.3.2c Influence of independent parameters on drug loading
3.3.3 Optimization and checkpoint analysis (validation of predicted values)
3.3.4 Physiochemical evaluation
3.3.4a Organoleptic evaluations
3.3.4b UV visible spectroscopy
3.3.4c Fourier transform infrared spectroscopy
3.3.4d X-ray diffraction
3.3.4e Thermogravimetric analysis
3.3.4f High-resolution transmission electron microscopy
3.3.4g Hydrodynamic size and zeta potential
3.3.4h Percent entrapment efficiency and drug loading
3.3.5 Storage stability
3.3.6 <i>In-vitro</i> drug release and kinetic model and mechanism
3.4 Animal studies
3.4.1 <i>In-vivo</i> pharmacokinetics
3.4.2 Histopathological studies
3.5 Conclusions
<b>Chapter 4: Synthesis of Methotrexate Chitosan Nanoparticles for Breast Cancer Treatment</b>
4.1 Introduction
4.2 Experimental section
4.2.1 Preparation of MTX-loaded chitosan nanoparticles
4.2.2 Physiochemical characterization of nanoparticles
4.2.3 Entrapment efficiency and loading capacity
4.2.4 Stability studies

4.2.5 Drug release studies
4.2.6 <i>In-vitro</i> studies
4.2.6a Cytotoxic studies
4.2.6b Detection of apoptosis; dual staining method employing acridine orange/ethidium bromide (AO/EBr)
4.2.6c Hemocompatibility studies
4.2.7 <i>In-vivo</i> Studies
4.2.7.1 Animal
4.2.7.1a Mammary tumor generation and treatment protocol
4.2.7.2 High-performance liquid chromatography
4.2.7.2a Pharmacokinetic studies
4.2.7.2b Biodistribution studies
4.2.7.3 Confocal laser scanning microscopy (Cellular Uptake)
4.2.8 Statistical analysis
4.3 Results and Discussion
4.3a Physicochemical characterization
4.3b Loading capacity and entrapment efficacy
4.3c Storage Stability
4.3.4 In-vitro drug release studies and kinetic models
4.3.5 Cytotoxic study of nanoparticle
4.3.5a MTT-Assay
4.3.5b Detection of apoptosis by acridine orange/ethidium bromide dual staining
4.3.6 Hemocompatibility studies
4.3.7 <i>In-vivo</i> pharmacokinetic and biodistribution
4.3.8 Anti-cancer efficacy
4.3.9 Confocal microscopy
4.4 Conclusions
<b>Chapter 5: Histopathological &amp; Biochemical Assessment using Developed Nano-formulation in Breast Cancer Rat Model</b>
5.1. Introduction
5.2 Experimental section
5.2.1 Animal grouping and treatment protocol
5.2.2 Assessment of cytokines as a biomarker (ELISA)

5.2.3 Assessment of renal and hepatic enzymatic function biomarkers
5.2.4 Histopathological study
5.2.5 Statistical analysis
5.3 Results and Discussion
5.3.1 Histopathology of mammary tumors (MNU-induced)
5.3.2 Role of pro-inflammatory cytokines in tumor generation
5.3.3 Role of MTX-loaded nanoparticles in tumor suppression
5.3.4 Role of Meth-Cs-NPs on hepatic & renal biomarker regulation
5.3.5 Tumor histology pathology (after treatments)
5.3.6 Effect of Meth-Cs-NPs on the kidney (histopathology)
5.3.7 Effect of Meth-Cs-NPs on the liver (histopathology)
5.4 Conclusion
<b>Chapter 6: Chitosan Functionalized Fluorescent Calcium Carbonate Nanocarrier Loaded with MTX as Unique Theragnostic Tool for Triple Negative Breast Cancer</b>
6.1 Introduction
6.2 Experimental sections
6.2.1a Plausible mechanisms for (@Cal-Nps synthesis
6.2.1b Surface modification of @Cal-Nps with chitosan and loading of methotrexate
6.2.2 Instrumentation & characterization
6.2.3 Loading capacity and entrapment efficiency
6.2.4 Stability study
6.2.5 Hemolysis assay
6.2.6 <i>In-vitro</i> drug release
6.2.7 <i>In-vitro</i> cell-line study
6.2.7a Cytotoxic study of nanoparticle
6.2.7b Apoptosis study through AO/EtBr dual staining
6.2.8 <i>In-vivo</i> anticancer efficacy
6.2.8.1 Animal grouping and treatment protocol
6.2.8.2 Pharmacokinetics study
6.2.8.3a Tissue biodistribution (Quantitative tissue biodistribution)
6.2.8.3b <i>In-vivo</i> fluorescent imaging (Qualitative tissue bio-distribution)

6.2.8.4 Enzyme-linked immunosorbent assays (ELISA)
6.2.8.5 Blood biomarker analysis
6.2.8.6 Tissue histology and immunohistochemistry (IHC) test
6.2.9 Statistical analysis
6.3. Results and Discussion
6.3.1 Synthesis of @Cal-Nps and loading capacity
6.3.2 Optical properties
6.3.3 Hydrodynamic particle size and zeta potential
6.3.4 Fourier transform infrared spectrophotometer analyses
6.3.5 High-resolution transmission electron microscopy & Selected area electron diffraction
6.3.6 Powder X-ray diffraction
6.3.7 Stability studies
6.3.7.1 Photostability
6.3.7.2 pH stability
6.3.7.3 Colloidal dispersion stability
6.3.7.4 Thermal stability
6.3.8 <i>In-vitro</i> drug release studies
6.3.9a Cytotoxic assay
6.3.9b Apoptosis study through AO/EtBr dual staining
6.3.10a Pharmacokinetics (PK) and tissue biodistribution
6.3.10b <i>In-vivo</i> optical imaging (IVIS)
6.3.11 Hemolysis assay
6.3.12 Anticancer efficacy
3.13 Enzyme-linked immunosorbent assays (ELISA)
6.3.14 Blood biomarker analysis
6.3.15 Immunohistochemistry (IHC) and histopathology
6.4 Conclusions
<b>Chapter 7: Summary &amp; Future Scope</b>
<i>References</i>
<i>Appendix</i>
<i>List of Publications</i>

## LISTS OF FIGURES

Figures no.	Figures caption
<b>Figure 1.1</b>	Worldwide cancer incidence and mortality rate.
<b>Figure 1.2</b>	a) Image represents the growth of hormonal receptors on the cell surface that express estrogen receptor (ER), progesterone receptor (PR), and, Human epidermal growth factor receptor 2 (HER-2), whereas b) Image indicates the absence of hormonal receptors on the cell surface (triple negative breast cancer).
<b>Figure 1.3</b>	Classification of Breast cancer. IDC: invasive ductal carcinoma.
<b>Figure 1.4</b>	Structure of methotrexate
<b>Figure 1.5</b>	Mechanism of action of Methotrexate
<b>Figure 1.6</b>	Limitation of the chemotherapeutic drug
<b>Figure 1.7</b>	Targeted drug delivery system used for breast cancer treatment.
<b>Figure 1.8</b>	Chemical Structure of chitosan
<b>Figure 1.9</b>	Various methods for synthetic chitosan nanoparticles
<b>Figure 2.1</b>	Schematic diagram of methotrexate delivery nanocarrier
<b>Figure 3.1</b>	Normal probability plot A) Particle size, B) Entrapment Efficiency, and C) % drug loading
<b>Figure 3.2</b>	S/N graph for Nanocarrier size (a), % Drug loading (b), and % Entrapment efficiency (c)
<b>Figure 3.3</b>	3D response surfaces (a, b, & c) and their corresponding 2D contour plot (d, e, & f) showing mutual interaction and discrete effects of different independent variables on nanocarrier size.
<b>Figure 3.4</b>	3D response surfaces (a, b, & c) and their corresponding 2D contour plot (d, e, & f) showing mutual interaction and discrete effects of independent variables on % entrapment efficiency.
<b>Figure 3.5</b>	3D response surfaces (a, b, & c) and their corresponding 2D contour plot (d, e, & f) show mutual interaction and discrete effects of independent variables on % drug loading.
<b>Figure 3.6</b>	Optimization plot of multiple responses
<b>Figure 3.7</b>	(a) Absorbance spectra and inset figure show UV-vis absorbance calibration curve of MTX, (b) FTIR spectra of chitosan, free MTX, and MTX-encapsulated chitosan nanocarrier (M-CNCs), (c) X-ray diffraction spectra for chitosan, free MTX, and M-CNCs and (d) TGA curve of M-CNCs.
<b>Figure 3.8</b>	a) Particle distribution curve using TEM image and b) HR-TEM image of Cs-NPs Nanoparticles.

<b>Figure 3.9</b>	Particles size and zeta potential graph of optimization nanocarrier
<b>Figure 3.10</b>	(a) Particles size, (b) PDI, (c) Zeta potential, (d) % Entrapment efficiency displays stability studies of nanoparticles at $4 \pm 2^\circ\text{C} / 60 \pm 5 \% \text{ (RH)}$ and $40 \pm 2^\circ\text{C} / 75 \pm 5 \% \text{ RH}$ .
<b>Figure 3.11</b>	In-vitro drug release studies at two different pH, results are expressed as the mean $\pm$ S.d (n=3).
<b>Figure 3.12</b>	In-vitro drug release data fitted into kinetic models; zero order, first order, Higuchi models, and Korsmeyer-Peppas; a,b, c, and d at pH 6.4, whereas e,f, g, and h at pH7.4.
<b>Figure 3.13</b>	Concentration–time profiles of MTX in blood plasma after iv administration of free MTX and M-CNCs. Results are expressed as the mean $\pm$ S.d (n=3).
<b>Figure 3.14</b>	Histopathological of the kidney and liver of the rats comparing the control group and those treated with M-CNCs at 7, 14, and 28 days revealed normal organ architecture and the absence of any noticeable tissue lesions.
<b>Figure 4.1</b>	The plausible crosslinking mechanism between chitosan and methotrexate (Ionic gelation process).
<b>Figure 4.2</b>	Schematic representation of Hemolysis protocol.
<b>Figure 4.3</b>	Schematic representation of tumor induction protocol.
<b>Figure 4.4</b>	Photograph of HPLC apparatus and Calibration curve for MTX using HPLC.
<b>Figure 4.5</b>	Schematic representation of Biodistribution procedure.
<b>Figure 4.6</b>	a) Particle size and b) Zeta potential of the Meth-Cs-Nps (with drug). Whereas c) Particle size and d) Zeta potential of the chitosan nanoparticles (without drug).
<b>Figure 4.7</b>	(a) FTIR spectra, (b) UV-vis absorbance spectra, (c) XRD pattern, (d) SEM image of Meth-Cs-NPs, (e) Particles size distribution curve for Meth-Cs-NPs, and (f) EDS analysis of Meth-Cs-NPs.
<b>Figure 4.8</b>	Stability studies of nanoparticles where; (a) Particle size, (b) Zeta potential, and (c) % EE at temperatures $25^\circ\text{C}$ and $40^\circ\text{C}$ .
<b>Figure 4.9</b>	(a) In-vitro drug release studies at pH 5.5 and 7.4, (b) Korsmeyer-Peppas kinetic model for Meth-Cs-NPs at pH 5.5, and (c) Korsmeyer-Peppas kinetic model at pH 7.4. Data represented; mean $\pm$ Sd (n=3).
<b>Figure 4.10</b>	Cytotoxic study of pure MTX, Cs-NPs, and Meth-Cs-NPs after 24 h incubation and Mechanism of action of MTX.
<b>Figure 4.11</b>	Morphology assessment of MDA-MB-231 cell after the treatment of nanoparticles where image A shows the control group of cells and B, C, and D represents a cells treatment group. Here white arrow shows live cells having maintained membrane integrity, while the red arrow shows early apoptotic cells have compromised the cell membrane. The yellow arrow shows late apoptotic cells.
<b>Figure 4.12</b>	(a) Hemolysis (%) of pure MTX and nanoparticles with red blood cells (RBCs). Where saline solution was employed as

	the negative control (NC), Triton X-100 as the positive control (PC), and (b) a Photograph of the tube after centrifugation. One-way ANOVA was used for the statistical analysis, followed by the Tukey post-test, where a significant difference from the control value is indicated by a * $P < 0.05$ . Data are presented as the mean $\pm$ S.d (n=3).
<b>Figure 4.13</b>	(a) Concentration–time profiles of MTX in blood plasma after iv administration of free MTX and MTX-Cs-NPs, and (b), (c) Biodistribution in various organs at 12 and 24 h after an i.v administration of free MTX and nanoparticles at an equivalent dose of 5 mg MTX/kg. Statistically significant differences from free MTX. *** $P < 0.001$ . Results are expressed as the mean $\pm$ S.d (n=3).
<b>Figure 4.14</b>	a) Shows Body weight before treatment, (b) Body weight after treatment, (c) Survival curve,(d) Tumor volume curve showed that the tumor growth was slower in Meth-Cs-NPs,(e) Tumor weight of different groups, (f) Tumor inhibition rate, One-way ANOVA followed by Tukey post-test analyzed results; All samples were compared with diseased control group a: Disease (control, untreated, b: Meth-Cs-NPs and c: Cs-NPs; (** $p < 0.001$ ), (** $p < 0.001$ ) and (* $p < 0.05$ ), (Data expressed as mean $\pm$ S.d, n =3).
<b>Figure 4.15</b>	Photograph of tumor-bearing rats and isolated tumors from different treatment groups.
<b>Figure 4.16</b>	Confocal image (cellular uptake); a & b are shown mammary tumors of the control group that showed less intensity with less cellular uptake (30 min), whereas c & d showed Nanoparticles with more intensity with high cellular uptake (60 min).
<b>Figure 5.1</b>	The strategy of ELISA (Enzyme-linked immunosorbent assays) working protocol and assessment of cytokines; Tumor Necrosis Factor- $\alpha$ and Interleukins (IL-1 $\beta$ & IL-6).
<b>Figure 5.2</b>	Histopathology of mammary tumors of rats (MNU-induced) indicates the tumor generation with different tissue morphology; (a) Normal mammary gland tissue; Epidermis (E), Dermis (D), Fat (F), and Connective tissue (C), (b) Intra-ductal proliferation or hyperplasia, (c) Solid comedocarcinoma in situ (DCIS): Distended ductal formations lined by a multilayered epithelium and centrally situated necrotic material with the intact basement membrane, and (d) In situ solid cribriform carcinoma: The basement membrane is still intact, and there are solid sheets of cancerous cells with irregularly formed secondary lumina within the lobule. H&E staining, bar size 1 $\mu$ m with 10X magnification.
<b>Figure 5.3</b>	Effect of Meth-Cs-NPs on pro-inflammatory cytokine. One-way ANOVA followed by Dunnett’s post-test analyzed results; All groups were compared with the normal control group. Where a; Normal control, b; Disease control, c; free

	MTX, d; Cs-NPs, and e; Meth-Cs-NPs. (**p < 0.001), (**p < 0.001) and (*p < 0.05). Data expressed as mean ± S.d, n =3.
<b>Figure 5.4</b>	The proposed mechanism of Methotrexate (MTX) blocks the primary enzyme dihydrofolate reductase (DHFR), which changes the dihydrofolate to tetrahydrofolate. The de novo synthesis of purines and pyrimidines and nuclear factor kappa B (NF-κB) activation were thought to be inhibited by MTX, which would result in the inhibition of cell proliferation (T & B) and cytokines expression. Inflammation, immunological response, cell proliferation, and apoptosis are regulated by the cytoplasmic transcription factor nuclear factor kappa B (NF-κB). The anti-inflammatory effects of MTX may be achieved by inhibiting NF-κB signaling. As a result, the cytokines, including TNF-α, IL-1β, and IL-6, were reduced when treated with nanoparticles.
<b>Figure 5.5</b>	The level of Biochemical markers in the serum of different groups. One-way ANOVA followed by Dunnett's post-test analyzed results; All groups were compared with the normal control group (NC). a; Normal control, b; Disease control (DC), c; free MTX, d; Cs-NPs and e; Meth-Cs-NPs. (**p < 0.0001), (**p < 0.001) and (*p < 0.05), (Data expressed as mean ± S.d, n =3).
<b>Figure 5.6</b>	Histopathology shows the mammary tumor of rat (MNU-induced) after treatment; (a) free MTX treated mammary tumor and (b) Meth-Cs-NPs treated mammary tumor. H&E staining, bar size 1μm with 10X magnification.
<b>Figure 5.7</b>	Histopathological of kidney section from control and different treatment groups; (a) Normal control, (b) Diseased control, (c) Free MTX, (d) Cs-NPs, (e) Meth-Cs-NPs treated groups. H&E staining, bar size 1μm with 10X magnification. GML; Glomerulus, BC; Bowman's capsule, PT; Proximal tubules, DT; Distal tubules.
<b>Figure 5.8</b>	Histopathological of liver section from control and different treatment groups; (a) Normal control group, (b) Diseased control group (multifocal mononuclear cell infiltrations indicated by black arrow), (c) Free MTX treatment group (mononuclear cell infiltration indicated by black arrow) (d) Cs-NPs treatment group and (e) Meth-Cs-NPs treatment group. H&E staining (Hematoxylin and Eosin) bar size 1μm with 20X magnification.
<b>Figure 6.1</b>	The fluorescence emission spectra of @Cal-Nps; a) the optimal excitation and emission spectra (λ <sub>EX</sub> 362 nm/λ <sub>EM</sub> 454 nm) of @Cal-Nps and (b) the excitation and emission spectra (λ <sub>EX</sub> 469 nm/λ <sub>EX</sub> 546 nm), c) the excitation and emission spectra (λ <sub>EX</sub> 516 nm/λ <sub>EX</sub> 581nm) and d) the excitation and emission spectra (λ <sub>EX</sub> 560 nm/λ <sub>EX</sub> 610 nm).

<b>Figure 6.2</b>	a) Particle size & b) zeta potential of the @Cal-Nps whereas c) Particle size & d) zeta potential of the @Cal-CS-Mtx-Nps
<b>Figure 6.3</b>	a) FTIR spectra, b) HR-TEM image, c) particles size distribution, d) SAED pattern of @Cal-Nps, and e) XRD spectra of @Cal-Nps
<b>Figure 6.4</b>	Stability study of @Cal-Nps: a) Photostability study of the @Cal-Nps under UV illumination at excitation wavelength 469 nm up to 120 min at a different time interval, b) pH-dependent fluorescent property of @Cal-Nps ( $\lambda_{\text{Ex}} = 469$ nm), c) thermogravimetric analysis of @Cal-Nps and d) Zeta potential values of @Cal-Nps at various time points.
<b>Figure 6.5</b>	a) Release profiles of Mtx from @Cal-Mtx-Nps and @Cal-CS-Mtx-Nps nanoparticles at pH = 5.5 and 7.4. Data are expressed as mean $\pm$ SD (n = 3), b) The cytotoxic assay of @Cal-NPs, Mtx, @Cal-Mtx-NPs, and @Cal-CS-Mtx-Nps against MDA-MB-231 cells. The statistical analysis was done by one-way ANOVA followed by the Tukey test, where * denotes a significant difference compared to the control.
<b>Figure 6.6</b>	Morphological assessment of MDA-MB-231 cells after the treatment of @Cal-CS-Mtx-Nps nanoparticles. Here white arrow shows live cells having maintained membrane integrity; the red arrow shows early apoptotic cells having compromised cell membranes, and the yellow arrow shows late apoptotic cells.
<b>Figure 6.7</b>	a) Mtx concentration in plasma release profile, b & c) tissue distribution plot and d) Photograph of isolated organ, e) Optical <i>In-vivo</i> fluorescent imaging of treatment group and Ex-vivo fluorescence images of isolated organs of tumor-bearing rats 24 h of post-injection of @Cal-Mtx-Nps and @Cal-CS-Mtx-NPs. IVIS images showing higher tumor tissue accumulation of @Cal-CS-Mtx-Nps as compared to @Cal-Mtx-Nps at 24 h after iv administration into tumor-bearing rats, f) %Hemolysis of @Cal-Nps with red blood cells (RBCs). Where saline solution was employed as the negative control (NC), Triton X-100 as the positive control (PC), and (g) a Photograph of the tube after centrifugation.
<b>Figure 6.8</b>	a) Experimental schedule for tumor induction and drug treatment, b) Body weight changes of rats as a function of days, b) Relative tumor volume curves of different groups after various treatments, c) tumor weight changes of rats as a function of days post-treatment for various groups d) relative tumor inhibition rat bar graph and e) Kaplan-Meier survival curve for different treatment groups, results show mean $\pm$ s.d (n =6).
<b>Figure 6.9</b>	Effect of Mtx on pro-inflammatory cytokine. One-way ANOVA followed by Dunnett's post-test analyzed results; All groups were compared with the normal control group

	(NC), Where; Disease control (DC), free Mtx, d; Cs-NPs, and e; Meth-Cs-NPs. (**p < 0.0001), (**p < 0.001) and (*p < 0.05). Data expressed as mean ± S.d, n =3.
<b>Figure 6.10</b>	The level of Biochemical markers in the serum of different groups. One-way ANOVA followed by Dunnett's post-test analyzed results; All groups were compared with the normal control group (NC). Normal control, Disease control (DC), free Mtx, @Cal-NPs, @Cal-Mtx-Nps and @Cal-CS-Mtx-Nps. The significant value p < 0.0001& non-significant values p > 0.05. Data expressed as mean ± S.d, n = 3.
<b>Figure 6.11</b>	Heterogeneity of triple-negative breast cancers; a) Normal mammary gland tissue, b) Invasive ductal carcinoma of no special type, c) Low magnification view of classic adenoid-cystic carcinoma, and d) Low magnification view of acinic cell carcinoma (ACC).
<b>Figure 6.12</b>	Immunohistochemistry (IHC) test; DMBA-induced breast tumor tissue and corresponding: ER staining, PR staining, and HER-2 staining. Pictures were taken with 10 & 20× magnification. The scale bar is 1 μm in length. ER, estrogen receptor; PR, progesterone receptor and HER-2, human epidermal growth factor receptor-2.
<b>Figure 6.13</b>	Histology of Kidney and live tissue from different treatment groups and normal rats; represent the H&E staining. Pictures were taken with 10X magnification with a scale bar is 1μm.

## LIST OF TABLES

Tables no.	Tables caption
<b>Table 2.1</b>	Summary of inorganic nanocarriers for methotrexate delivery
<b>Table 2.2</b>	Benefits and limitations of inorganic nanomaterials for cancer treatment.
<b>Table 2.3</b>	Summary of organic nanocarriers for methotrexate delivery
<b>Table 3.1</b>	Selected factors at three different levels and the responses
<b>Table 3.2</b>	Taguchi design (DOE) L9 (3 ^ 3) orthogonal array
<b>Table 3.3</b>	ANOVA for Nanocarrier Size (Y1)
<b>Table 3.4</b>	ANOVA for % Entrapment Efficiency (Y2).
<b>Table 3.5</b>	ANOVA for % Drug loading (Y3).
<b>Table 3.6</b>	Optimized formulation batch of Methotrexate-encapsulated chitosan nanocarrier with a predicted and experimental response with its relative error
<b>Table 3.7</b>	Nanocarrier size, PDI, and Zeta potential of M-CNCs
<b>Table 3.8</b>	Long-term Storage stability of M-CNCs at 4°C and 40°C
<b>Table 3.9</b>	In-vitro drug release kinetic models fit for free MTX and M-CNCs with the regression coefficient.
<b>Table 3.10</b>	Pharmacokinetic parameter of free MTX and M-CNCs in plasma of rats after intravenous administration of the equivalent dose of 5 mg/kg of MTX
<b>Table 4.1</b>	Particle size, PDI and zeta potential, % EE and % LC of the nanoparticles
<b>Table 4.2</b>	Stability studies for Meth-Cs-NPs at two different temperatures
<b>Table 4.3</b>	The shape parameter of the release kinetics
<b>Table 4.4</b>	The value of regression coefficient ( $r^2$ ) for release kinetics models.
<b>Table 4.5</b>	Pharmacokinetic parameters of free MTX and Meth-Cs-NPs at a 5 mg MTX/kg dose in blood plasma after i.v administration
<b>Table 4.6</b>	Amount of MTX in different tissue of rats after an i.v injection of drug and MTX-NPs at an equivalent dose of 5 mg MTX/kg
<b>Table 5.1</b>	Effect of MTX on pro-inflammatory cytokines levels in treatment groups.
<b>Table 5.2</b>	Effect of MTX on biochemical marker levels in experimental groups.
<b>Table 6.1</b>	Pharmacokinetic (PK) parameter in rats in plasma after i.v injection of the equivalent dose of 5 mg/kg of Mtx
<b>Table 6.2</b>	Effect of methotrexate on pro-inflammatory cytokines levels in various treatment groups.
<b>Table 6.3</b>	Effect of methotrexate on blood biomarker levels.

---

## ABBREVIATION

ANOVA	One-way Analysis of Variance
AUC	Area under the concentration-time curve
ALP	Alkaline Phosphate
BSC	Biopharmaceutical Classification System
BSA	Bovine Serum Albumin
BC	Breast Cancer
CS	Chitosan
CS-NPs	Chitosan Nanoparticles
C <sub>max</sub>	Maximum plasma concentration
CL	Plasma Clearance
DOE	Design of Experiments
DL	Drug Loading
DMSO	Dimethyl Sulfoxide
DMEM	Dulbecco Modified Eagle Medium
DMBA	7,12-Dimethylbenz[a]anthracene
DLS	Dynamic Light Scattering
EE	Entrapment Efficiency
ELISA	Enzyme-Linked Immunosorbent Assays
ER	Estrogen Receptor
FTIR	Fourier Transform Infrared Spectroscopy
FBS	Fetal Bovine Serum
HR-TEM	High-Resolution Transmission Electron Microscopy
HPLC	High-Performance Liquid Chromatography
HER-2	Human Epidermal Growth Factor Receptor 2
IVIS	In-vivo Fluorescent Imaging
IL	Interleukins
IHC	Immunohistochemistry
i.p	Intraperitoneally injection
i.v	Intravenous injection
KBr	Potassium Bromide
MTX	Methotrexate

MTT	3-(4, 5-dimethylthiazol-2-yl)-2,5 diphenyl tetrazolium bromide
MRT	Mean Residence Time
NMU/MNU	N-methyl N-nitrosourea
NPs	Nanoparticles
PBS	Phosphate buffer solution
PDI	Polydispersive Index
PK	Pharmacokinetic
P/CL	Polymer/cross-linker ratio
PR	Progesterone Receptor
RSM	Response Surface Methodology
RT	Reaction Time
SAED	Selected Area Electron Diffraction
SEM	Scanning Electron Microscope
s.d	Standard deviation
S/N ratio	Signal-to-Noise ratio
SD	Sprague Dawley
STPP	Sodium tripolyphosphate
SGOT/ALT	Serum Glutamic Oxaloacetic Transaminase
SGPT/AST	Serum Glutamic Pyruvic Transaminase
t <sub>1/2</sub>	Plasma half-life
TNBC	Triple Negative Breast Cancer
TNF- $\alpha$	Tumor Necrosis Factor- $\alpha$
TGA	Thermogravimetric Analysis
Vd	Volume of distribution
XRD	X-Ray Diffraction

---

## PREFACE

We successfully synthesized methotrexate-loaded chitosan nanoparticles in this study using the ionic gelation method. Taguchi design was employed to optimize formulation parameters such as particle size, entrapment efficiency, and drug loading capacity. The nanoparticles were designed to improve therapeutic efficacy and minimize the side effects of methotrexate in breast cancer treatment. Additionally, we developed a self-targeted formulation by modifying reaction conditions. Also, we synthesized fluorescent calcium carbonate nanoparticles functionalized with chitosan and loaded them with methotrexate for controlled drug delivery. The nanoparticles were extensively characterized using various techniques, including UV-vis spectrophotometry, HPLC, DLS, FTIR, XRD, SAED, fluorescence spectrophotometry, IVIS, and biochemical analysis. The nanoparticles exhibited spherical morphology and demonstrated good biocompatibility and anticancer effects. They effectively reduced cytokine levels and showed high potential for triple-negative breast cancer treatment. The optimized nanoparticles had desirable physicochemical properties, controlled drug release, and improved pharmacokinetic profiles compared to free methotrexate. They exhibited biocompatibility, minimal hemolysis, and higher cytotoxicity against breast cancer cells. In a chemically-induced breast cancer rat model, the nanoparticles significantly inhibited tumor growth compared to free methotrexate. These findings highlight the potential of the developed nanoparticles for breast cancer treatment, offering enhanced drug delivery, improved pharmacokinetics, and reduced toxicity. The functionalized fluorescent nanoparticles also demonstrated biocompatibility, bioimaging capabilities, and anticancer activity. This study provides a promising therapeutic approach with the potential for clinical translation in the future. The thesis work has been conceptualized considering the above-discussed aspects of biocompatible nanocarrier research for breast

---

cancer treatment. The thesis consists of seven chapters, with the first two devoted to the introduction, literature review & the objective of the work section. Four out of the remaining five chapters extensively discussed different aspects of prepared nanoparticles and their application in breast cancer treatment. The last chapter belongs to the summary of the overall research.

The present study is divided into the following chapters.

**Chapter 1:** This chapter provides an in-depth exploration of cancer, including its various types, prevalence, and the urgent need for effective treatment strategies. It highlights the wide-ranging prospects of nanoparticles in the context of breast cancer treatment, emphasizing their potential to revolutionize current therapeutic approaches. The chapter delves into the crucial considerations involved in material selection for nanoparticle synthesis, considering the desired properties and characteristics necessary for effective drug delivery. Furthermore, it discusses the adopted technologies employed during the synthesis of nanoparticles, focusing on the ionic gelation method and its advantages. Special emphasis is given to the superiority of polymeric nanoparticles and inorganic nanomaterials, discussing the unique properties that make them ideal candidates for targeted drug delivery and enhanced therapeutic outcomes in breast cancer treatment.

**Chapter 2:** In this chapter, exploring the comprehensive review critically examines the potential of Methotrexate-loaded or encapsulated chitosan-based nanoparticles for breast cancer treatment. It covers various aspects, including synthesis techniques, physicochemical characterization, drug release kinetics, cellular uptake mechanisms, and strategies to enhance therapeutic efficacy. This comprehensive analysis serves as a foundation for further research and development in the field of chitosan-based nanoparticle formulations for breast cancer therapy.

---

**Chapter 3:** This chapter focuses on synthesizing a 1-hour-methotrexate-encapsulated polymeric nanocarrier using the ionic gelation method. The formulation is optimized using Taguchi design, a Design of Experiment (DOE) approach, to enhance its effectiveness in improving therapeutic efficacy while minimizing the side effects of the drug. The chapter delves into the details of the synthesis process, discussing the specific parameters and conditions employed to achieve the desired nanocarrier formulation. To ensure the reliability and quality of the nanocarrier, a comprehensive characterization is conducted using various microscopy and spectroscopy techniques. Furthermore, the chapter addresses the crucial aspect of assessing the toxicity of the nanocarrier. To evaluate its safety, a toxicity study is conducted in normal rats, with the evaluation focusing on tissue histopathology analysis.

**Chapter 4:** This chapter focuses on formulating a single-step self-assembly 3-hour-methotrexate-encapsulated polymeric nanocarrier that exhibits pH-sensitive drug release specifically designed for the breast cancer microenvironment. To evaluate the anticancer efficacy of the nanoparticles, a chemically induced N-methyl-N-nitrosourea (NMU) breast tumor rat model is developed. Furthermore, the assessment includes evaluating tumor volume, tumor weight, and other relevant parameters to determine the therapeutic impact of the nanoparticles on breast cancer.

**Chapter 5:** This chapter described the histopathological and biochemical assessment using a developed nano-formulation chemically N-methyl-N-nitrosourea (NMU) induced breast tumor rat model. Histopathology was done for tumor tissue, Kidney, and liver to check any toxicity of nanoparticles. Nano-formulation intravenous administrated in tumor-bearing rats, liver and kidney biomarker analysis was done. And different pro-inflammatory cytokines such as TNF- $\alpha$ , IL-1 $\beta$ , and IL-6 were also checked for tumor generation confirmation and treatment efficacy.

---

**Chapter 6:** This chapter focuses on synthesizing chitosan-functionalized luminescent calcium carbonate nanoparticles (@Cal-CS-MTX-Nps) as a carrier for methotrexate and uses it for bioimage and treatment in breast tumor-bearing rats. The nanoparticles were characterized by various spectroscopy and microscopy techniques. The anticancer efficacy of nanoparticles was assessed in DMBA (dimethylbenz (a) anthracene) induced breast tumor rat model.

**Chapter 7:** The final chapter summarizes the overall research findings and provides conclusions regarding the development and application of methotrexate-loaded chitosan nanoparticles for breast cancer treatment.